Vicenzi *et al. Herit Sci (2016) 4:26*
DOI 10.1186/s40494-016-0093-2

Heritage Science

RESEARCH ARTICLE

Open Access

Rock varnish on architectural stone: microscopy and analysis of nanoscale manganese oxide deposits on the Smithsonian Castle, Washington, DC

Edward P. Vicenzi[1*], Carol A. Grissom[1], Richard A. Livingston[2] and Zoe Weldon-Yochim[1]

Abstract

The Smithsonian Institution Building, commonly referred to as the Castle, is located on the National Mall in Washington, DC, and was constructed in the mid-nineteenth century for the purpose of housing all museum and scientific functions for the newly formed institution. Matching gateposts designed by the Castle's architect were erected more than a century later in the Enid A. Haupt Garden opposite the Castle. Black patches were recently noted on both structures, which are clad with locally quarried Seneca red sandstone. Portable x-ray fluorescence (XRF) spectrometry links the discoloration with elevated Mn concentrations. The discolored patches resemble rock varnish, a Mn-rich coating observed on rock surfaces formed in a variety of environments. Bulk rock and varnish chemistry, in addition to microscopy and microanalysis of the varnish, are presented here. On a bulk chemical basis, the Seneca sandstone is relatively poor in Mn, containing ~500 ppmw. In contrast, the rock varnish is greatly enriched in Mn relative to the stone and to a lesser degree in Pb, Ca, Zn, Cu and Ni. Cross sections of the black encrusted regions show that the stone's red coloration has been modified by black pigmentation from the surface down to ~250 µm. X-ray diffraction of blackened particles produced no discernable pattern, indicating concentrations below the detection limit, poor crystallinity, or both. Scanning electron microscopy and EDS-based x-ray microanalysis of the uppermost portion of the cross section reveal nanometer scale (<20–200 nm) Mn-rich and clay particles concentrated in a thin film (≪1 µm) at the surface. Additionally, Mn oxide particles decorate the surfaces of fine-grained minerals in sandstone pores within the discolored zone. Imaging and microanalysis of the rock surface reveal that the Mn-rich varnish is a discontinuous film ≪1 µm in thickness with an estimated composition of $Na_{0.2}Ca_{0.1}Mg_{0.1}Al_{0.1}Si_{0.5}Mn_{1.9}Fe_{0.5}O_{6.7}$. This composition most likely represents a nanoscale mixture of a Mn oxide (e.g., birnessite or todorokite) and an Al-rich silicate mineral. Seneca sandstone on the Smithsonian Castle and gateposts is discolored in patches owing to the Mn-rich phase being deposited into two zones: (1) a vanishingly thin patina, and (2) nanoparticles coating grain boundaries and pores in the uppermost ~200–250 µm of the stone. While the mineralogy is similar to well-studied varnish formed in arid settings, rock varnish on the Smithsonian structures is significantly thinner. Because this architectural rock varnish is young, it may represent the earliest stages of formation of the more commonly described varnishes reported in the literature.

Keywords: Building stone, Desert varnish, Microanalysis, Nanophase, Sandstone, Stone conservation, SEM, XRF

*Correspondence: Vicenzie@si.edu
[1] Smithsonian Institution, Museum Conservation Institute, 4210 Silver Hill Road, Suitland, MD 20746, USA
Full list of author information is available at the end of the article

Background

The Smithsonian Institution Building, more commonly referred to as the Castle, was designed by architect James Renwick Jr. in medieval revival style (Fig. 1). The building was sited on the National Mall, and construction was completed in 1855. As the first Smithsonian building, the Castle housed chemical laboratories, exhibit halls, specimen storage, and all other institution functions, as well as the residence and office for physicist Joseph Henry, the first Secretary of the institution [1, 2]. It is clad with Seneca red sandstone quarried from the Bull Run Quarry at Seneca, Maryland, located 40 km northwest of the city [3, 4]. The Seneca sandstone was selected after frost testing of 25 building stones by Charles G. Page [4]. Also made from the Seneca sandstone are gateposts designed by Renwick, but erected only in 1987 opposite the Castle in the Enid A. Haupt Garden, mainly from stone salvaged from the former DC Jail (1872), which was demolished in 1982 (Fig. 2). Seneca sandstone is described as an arkosic micaceous sandstone. Stratigraphically it is part of the Poolesville Member of the Manassas Sandstone of late Triassic age. Manassas Sandstone is in turn a Member of the Newark Supergroup, which provided large quantities of brownstone for New York and other east coast US cities during the latter half of the 19th century. In an 1847 report on the quality of the recommended sandstone, geologist Dr. David Dale Owen stated that the Seneca sandstone is resistant to

> *"atmospheric vicissitudes, (and) even the most severe mechanical wear and tear." [5]*

Black or blue black patches were photographed on the Castle and Haupt Garden gateposts beginning in 2007, but the hypothesis that it was related to rock varnish was not made until 2013. Field measurements using portable x-ray fluorescence (XRF) spectrometry linked the discoloration with elevated Mn concentrations [6]. This discovery was confirmed by energy dispersive x-ray spectrometry (EDS) in the SEM [6]. The facades of other red Seneca sandstone buildings in Washington, DC, suffer similar disfiguring black patches, e.g., Oak Hill Cemetery gateposts (1850), also designed by Renwick, and the Cathedral of St. Matthew the Apostle (1893).

The black discoloration is best described as rock varnish, a thin dark coating on rock surfaces found in all environments but most easily noticed in arid settings where unvegetated geological features prominently stand out [7]. Varnishes are heavily enriched in Mn relative to the rocks they coat, and previous investigations have determined their mineralogy [8–10] and outlined the evidence for microbial activity in several rock varnishes [11]. Desert varnish study is an active discipline given its relevance to paleoclimate research [12, 13]; prehistoric artifacts and the history of petroglyph surfaces [14, 15]; and its potential application to astrobiology and planetary environments [16].

Fig. 1 The Smithsonian Institution Building (1847–1855), aka "The Castle," viewed from the southwest in 2015. Situated on the National Mall in Washington, DC, the Castle is located midway between the United States Capitol and the Washington Monument

Fig. 2 Enid A. Haupt Garden gateposts with the Castle in the background. *Inset*: drawing depicts locations of rock varnish on the gateposts

To the best of our knowledge this study represents the first significant examination of rock varnish on architectural stone. Hand specimen analysis by XRF, scanning electron microscopy, and detailed x-ray microanalytical tools have been used to characterize the rock varnish found on the Smithsonian Castle and gateposts in Washington, DC.

Methods

Instrumental neutron activation analysis

Bulk chemistry was determined by instrumental neutron activation analysis (INAA) at the University of Missouri Research Reactor Center. Established standardization and analysis methods [17] were used to determine elemental concentrations, including an interference correction for aluminum fast neutrons on magnesium. Because silicon was not determined directly, silica was computed by subtracting the sum of all measured oxides from 100. Therefore, these silica values are subject to considerable uncertainty given that other elements, e.g., H and P, were not measured by INAA.

Portable x-ray fluorescence

Major, minor, and trace elements were analyzed using a Bruker Tracer III-SD hand-held x-ray fluorescence (XRF) spectrometer. A rhodium x-ray source with an energy of 40 kV, beam current of 20 μA, and an x-ray spot size of ~5 mm was used to collect x-ray spectra for 120 live seconds. The Bruker yellow filter, 0.001″ Ti plus 0.012″ Al, was used to reduce background intensity in the energy region of interest. The silicon drift detector (SDD) operated with dead times less than approximately 10 %. The x-ray continuum was subtracted, and corrections for interfering peaks (e.g., Mn K_β on Fe K_α) in reporting elemental net intensities were determined for XRF spectra using Bruker Artax data evaluation software v7.2.5.

Scanning electron microscopy and x-ray microanalysis

Scanning electron microscopy and EDS-based x-ray microanalysis were conducted using three instruments: (1) an FEI Nova NanoSEM 600 field emission SEM equipped with a 40 mm^2 Thermo Scientific NanoTrace SiLi x-ray detector, (2) an Hitachi S3700N tungsten source SEM equipped with a 10 mm^2 Bruker XFlash 4010 SDD, and (3) an FEI Quanta 200F field emission SEM equipped with a 30 mm^2 Bruker XFLash 5030 SDD. Polished cross sections were carbon coated and examined at 12.5 kV at lower resolution and 7 kV for higher spatial x-ray resolution work on the NanoSEM 600 and Hitachi S3700N. Uncoated rock varnish surfaces were imaged at 10 and 13 kV under variable pressure conditions (~0.7 mbar P_{H2O}). These surfaces were then carbon coated and analyzed under high vacuum at 7 kV. X-ray spectra were extracted from hyperspectral data sets and analyzed using Thermo Scientific NSS v 3.2 for polished cross sections and Bruker Esprit v 1.9.4 software packages for rough surfaces. Multivariate statistical analysis of hyperspectral data cubes were performed using NSS COMPASS, which is based upon research performed at Sandia National Laboratories [18, 19]. The interactive

peak/background ZAF correction routine was utilized in Bruker Esprit to minimize the effect of rough surfaces on compositional microanalyses.

X-ray diffraction

A Rigaku D/MAX RAPID micro-x-ray diffractometer equipped with a semicylindrical imaging plate was utilized for identification of crystalline materials in the rock varnish. Mineral fragments extracted from the rock surface heavily coated with fine-grained black material were selected for x-ray diffraction pattern collection.

Results

Disposition of rock varnish

Irregular black or blue–black patches, measuring as large as 80 cm in long dimension, can be documented on the Castle edifice beginning only in the mid-1990s based on limited photographic documentation of sufficient detail. In 2015 this rock varnish was documented on every face of the building, with the heaviest concentration on the south façade (Fig. 3). The discolored zones are numerous on most façades and are not regularly arranged, nor do they appear to follow either water drainage or soiling patterns (Fig. 4). They are also apparent on the Haupt Garden gateposts, mainly on south faces (Fig. 2). Most patches occur within single blocks, but some span several blocks and are found on mortar in between, as well as on mortar repairs.

Bulk rock and varnish chemistry

The bulk chemical composition of Seneca sandstone used to construct the Castle and the Enid A. Haupt Garden gateposts (DC Jail) was determined by instrumental neutron activation analysis (INAA), and results are presented in Table 1 [20]. The two stones are similar in major element composition, although Fe is ~14 % greater in concentration for the Castle compared to DC Jail stone. Most notably, Mn is present at trace element concentrations for both sandstones. Of further note is that Fe is enriched in the bulk relative to Mn by a factor of ~100.

Samples of rock varnish were taken from the Haupt Garden gateposts for imaging and analysis in this study for multiple reasons: (1) ease of access, (2) exfoliation of thin layers with rock varnish, making them easy to pry from the stone (Fig. 5a), and (3) a clear time line for rock varnish formation at a relatively youthful sandstone-atmosphere interface. In this study gatepost samples, rather than those from the main building, have been subjected to detailed examination but are referred to as Smithsonian Castle varnish. For the purposes of the following discussion the terms Smithsonian Castle varnish and rock varnish are used interchangeably.

Portable XRF spectra taken from the Smithsonian Castle varnish surface necessarily include chemical information from bulk sandstone given the thin layer of varnish (Fig. 5b) compared to the greater penetration depth of x-ray generation and detection. A comparison of the ratio of the combined varnish plus sandstone to the sandstone interior spectra reveals that the rock varnish is enriched in the following metals (Fig. 6):

$$\mathrm{Mn} \gg \mathrm{Pb} > \mathrm{Ca},\ \mathrm{Zn},\ \mathrm{Cu},\ \text{and}\ \mathrm{Ni}$$

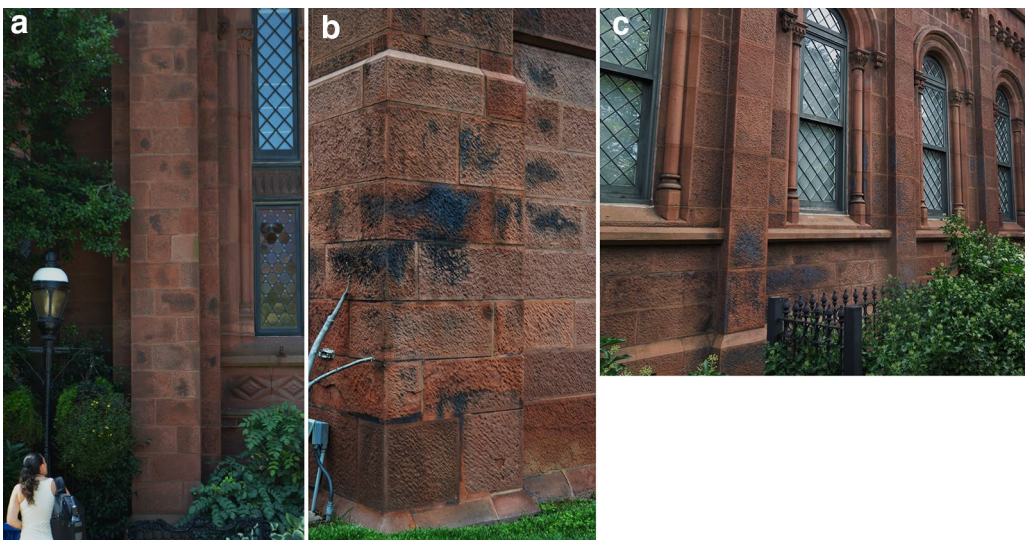

Fig. 3 Rock varnish on the Castle's Seneca sandstone and mortar. **a** Buttress adjacent to the porte cochere, north façade. **b** Southwest corner. **c** West façade

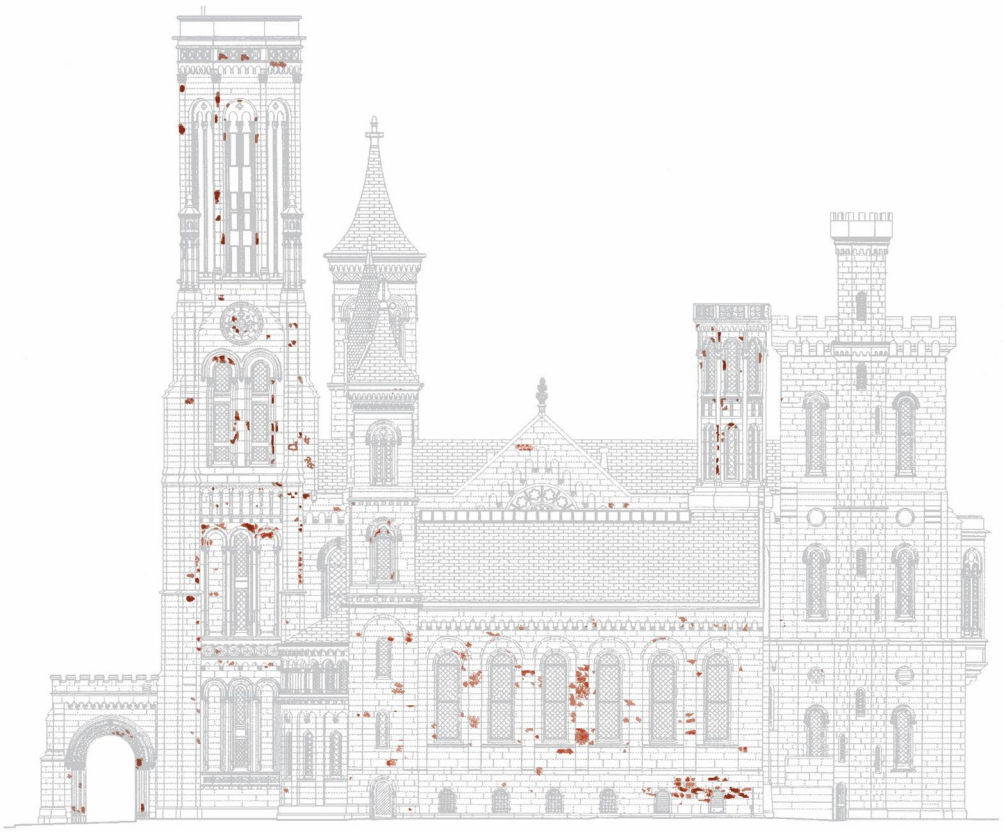

Fig. 4 West architectural elevation of the Castle showing rock varnish. An estimate of the areal distribution of Mn-bearing rock varnish on the building in 2015 is represented by *red-brown* patches

Table 1 INAA bulk chemistry for architectural Seneca sandstone used for two Washington, DC structures expressed as weight per cent

Oxide/El	$Castle_1$	$Castle_2$	$Castle_{avg}$	$DC\ jail_1$	$DC\ jail_2$	$DC\ jail_{avg}$	$Overall_{avg}$
SiO_2[a]	56.26	53.36	54.81	57.76	57.40	57.58	56.20
Al_2O_3	22.94	25.05	24.00	23.21	23.26	23.24	23.62
CaO	0.58	0.64	0.61	0.33	0.23	0.28	0.45
MgO	0.16	0.20	0.18	0.00	0.00	0.00	0.09
Fe_2O_3[b]	6.15	6.53	6.34	4.57	4.61	4.59	5.47
K_2O	2.83	2.91	2.87	3.26	3.84	3.55	3.21
Na_2O	10.22	10.41	10.32	10.12	9.92	10.02	10.17
TiO	0.75	0.78	0.77	0.62	0.62	0.62	0.69
MnO[c]	0.04	0.04	0.04	0.06	0.05	0.06	0.05
Fe	4.30	4.57	4.43	3.20	3.22	3.21	3.83
Mn	0.03	0.03	0.03	0.05	0.04	0.05	0.04
Fe/Mn	138.76	147.43	143.14	68.79	83.27	69.09	98.80

[a] Computed by difference; 100-Σall measured oxides (note: H and P not measured)

[b] Total iron expressed as Fe^{3+}

[c] Total manganese expressed as Mn^{2+}

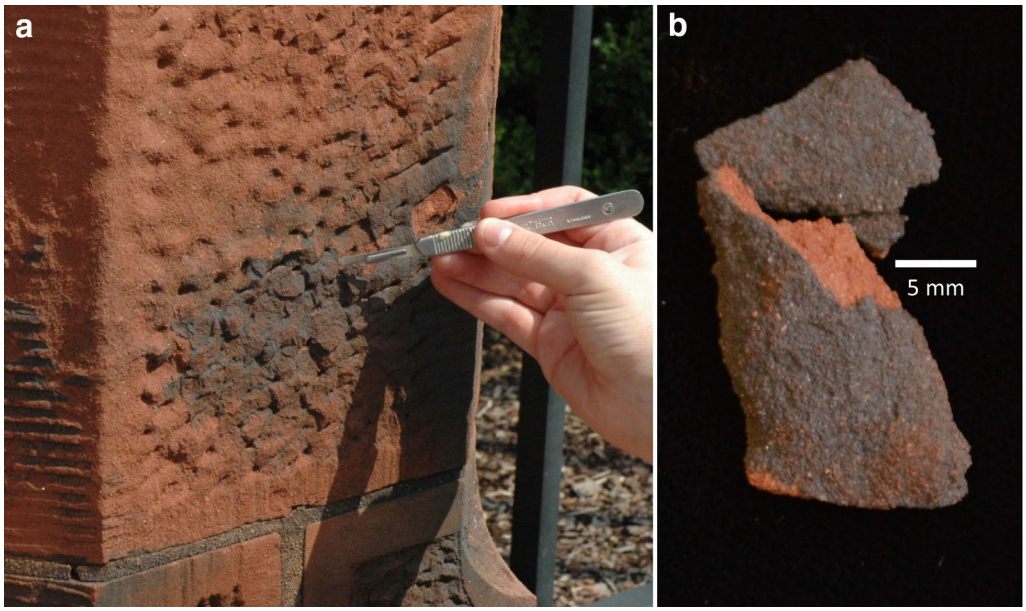

Fig. 5 Close-up view of rock varnish. **a** Sampling a garden gatepost for microscopy and analysis. **b** Hand specimen image of removed surface flake showing *marked color* contrast between the red bulk rock and varnish

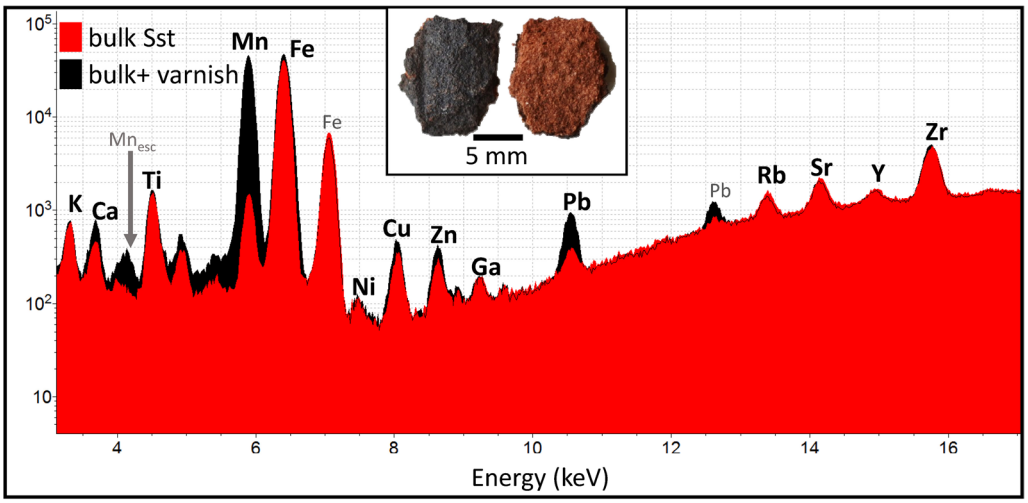

Fig. 6 Portable x-ray fluorescence spectra of a gatepost surface flake with rock varnish. XRF spectral comparison of the bulk sandstone (Sst) versus rock varnish + bulk spectrum. The *grey arrow* marks a spectral artifact in the *black* spectrum at 4.16 keV caused by the escape peak for Mn Kα.The large dynamic range of XRF data requires a log scale plot. *Inset* hand specimen images of the flake exterior (*left*) and interior fracture surface (*right*)

Other elements (K, Ti, Fe, Rb, Sr, Y, and Zr) are within 10 % of unity for the above ratio (Table 2). The lone exception is Ga, which is depleted in the varnish, yet this peak has the fewest net counts and is therefore subject to the greatest uncertainty. Because the distinctive x-ray signal from the varnish has an interaction volume greater than that layer, it is diluted by unaltered underlying sandstone. As a result, the portable XRF enrichment/depletion net intensity ratios listed in Table 2 represent minimum estimates.

An attempt was made to characterize samples using micro x-ray diffraction to precisely identify the mineralogical assemblage of the rock varnish. Despite careful specimen selection and lengthy acquisition times, the x-ray diffraction patterns obtained reflected the substrate minerals only, with no additional information regarding the varnish phase(s).

Table 2 Portable x-ray fluorescence spectrometry net intensity results for rock varnish and fresh fractured Seneca sandstone surfaces shown in Fig. 6

Element/ net intensities	X-ray line	$Black_1$	$Black_2$	Black B_{avg}	Red_1	Red_2	Red R_{avg}	B_{avg}/R_{avg}
K	K_α	3604	3089	3347	2960	3542	3251	1.03
Ca	K_α	3765	3210	3488	1883	1955	1919	*1.8*
Ti	K_α	10,788	9928	10,358	10,474	10,302	10,388	1.00
Mn	K_α	357,188	328,229	342,709	4992	10,533	7763	*44.15*
Fe	K_α	360,371	333,692	347,032	319,972	328,254	324,113	1.07
Ni	K_α	382	376	379	256	301	279	*1.4*
Cu	K_α	3363	3212	3288	2119	2261	2190	*1.5*
Zn	K_α	2676	2596	2636	1428	1614	1521	*1.7*
Ga	K_α	324	–	162	563	555	559	0.3
Rb	K_α	6221	5948	6085	6606	7420	7013	0.9
Sr	K_α	12,303	11,791	12,047	12,317	13,234	12,776	0.9
Y	K_α	4643	4264	4454	4442	4430	4436	1.00
Zr	K_α	44,471	39,197	41,834	41,126	39,503	40,315	1.04
Pb	L_α	7753	8219	7986	1403	1565	1484	*5.4*
Fe/Mn		1.009	1.017	1.013	64.10	31.16	41.8	

Elements significantly enriched in the varnish (B_{avg}/R_{avg}) in italics

Varnish in cross section

An image of a polished cross section of varnish flake removed from a gatepost reveals the uniform red color of the Seneca sandstone interior. Loss of red color occurs in the uppermost 0.2–0.25 mm darkened zone though the thickness of this layer is somewhat variable (Fig. 7). Absence of red in this layer is likely due to the strong pigmentation of the Mn-rich phase.

A detailed examination of the cross section using SEM imaging and x-ray microanalysis reveals that Mn is found throughout the discolored layer. However, Mn is particularly enriched in the uppermost 100 µm or so, and the density of Mn-bearing particles tails-off precipitously with depth from the rock surface (Fig. 8a).

In terms of mineralogical make-up, the most abundant detrital grains in this section of the Seneca sandstone are quartz, plagioclase feldspar, alkali feldspar, and micas. Accessory minerals rich in first row transition metals, e.g. hematite (Fe_2O_3), titanite ($CaTiSiO_5$), and rutile (TiO_2) are present at minor to trace volumes. While these minerals typically contain minor Mn, SEM-based compositional imaging reveals no pattern of Mn migration from these interior grains to the rock surface.

The smallest Mn-rich particles are not resolvable using an SEM, but it can be stated that the size distribution ranges from <20 nm to rarer larger particles roughly 200 nm in size (Fig. 8b). The composition of Mn-rock varnish cannot be unambiguously determined in cross section owing to the size of the particles (10 s of nm) and the x-ray interaction volume produced by the electron beam (100 s of nm) at low energy. Nevertheless, multivariate statistical analysis of hyperspectral x-ray imaging

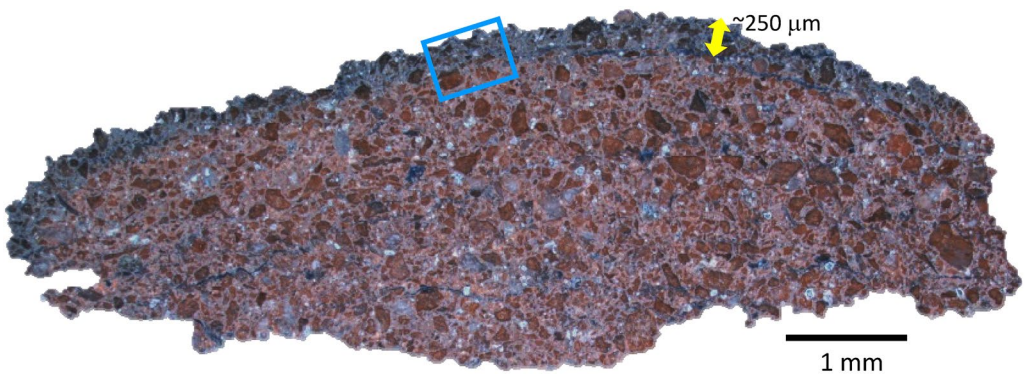

Fig. 7 Visible light image of polished cross section with rock varnish. The darkened zone is estimated to be roughly 200–300 µm in depth from the stone surface

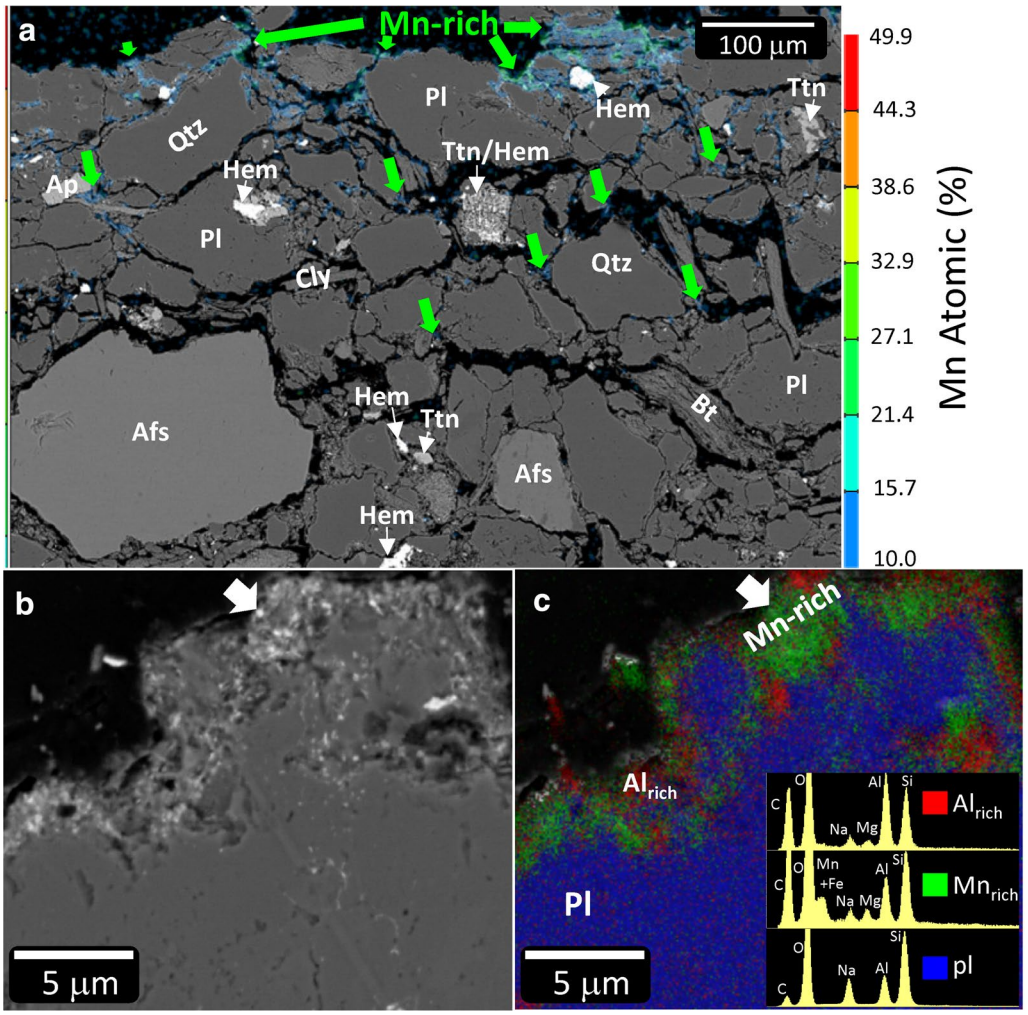

Fig. 8 SEM-based x-ray microanalysis of rock cross sections with rock varnish. **a** Quantified Mn map (threshold >10 atom%) superimposed on backscattered electron (BSE) image of highlighted region in Fig. 7. *Qtz* quartz, *Pl* plagioclase feldspar, *Afs* alkali feldspar, *Bt* biotite, *Ttn* titanite, *Hem* hematite, *Cly* clay and *Ap* apatite. **b** Higher resolution BSE image of a cross section at the rock surface where Mn is concentrated. **c** RGB overlay of previous with multivariate statistical (MVS) components that model the hyperspectral x-ray data set. *Inset*: Component spectra associated with *red* (Al-rich phase), *green* (Mn-rich phase), and *blue* (plagioclase) component images

results shows that rock varnish is composed of two components: (1) a Mn-rich phase with a Mn/Fe ratio of ~2 (Table 3), and (2) an Al-rich phase with Al/Si ratio of ~1, which is not inconsistent with clay (Fig. 8c; Table 3). In addition to deposits at the stone-atmosphere interface, nanoscale Mn particles also decorate the grain boundaries of fine grained material within sandstone voids (Fig. 9a, b, d) and along grain boundaries (Fig. 9c).

Surface imaging and analysis

Characterizing the uncoated rock varnish surface using variable pressure (VP)SEM imaging reveals the discontinuous nature of the environmental patina on the Seneca sandstone at the millimeter scale (Fig. 10a). Moderate magnification imaging shows that most grain boundaries intersecting the rock surface are covered with a film, while some larger flat areas remain uncoated (Fig. 10b). Morphological imaging of the rock varnish surface can be described as an agglomeration of nanometer scale particles (Fig. 11).

Electron imaging of the surface coupled with compositional imaging shows that Mn-enriched zones form lacy 2D networks (Fig. 12a, b). These deposits are clearly discontinuous in nature and are usually heavily enriched in Mn relative to Fe (Fig. 13). Extraction of x-ray spectra exclusively from Mn-rich regions yields an estimate of the major and minor element chemistry of the Seneca sandstone rock varnish (Table 4). The average composition expressed in terms of atomic fraction is:

$$Na_{0.2}Ca_{0.1}Mg_{0.1}Al_{0.1}Si_{0.5}Mn_{1.9}Fe_{0.5}O_{6.7}$$

Table 3 EDS-based x-ray microanalyical results for component spectra shown in Fig. 8c

Oxide	Al-rich	Mn-rich	Plagioclase
SiO_2	49.3	22.0	62.2
Al_2O_3	43.4	9.9	17.6
CaO			
MgO	2.9	2.0	
$Fe_2O_3^b$		23.5	0.0
K_2O			0.1
Na_2O	4.4	1.8	10.4
MnO^c		40.8	9.6
Oxygens	10	10	8
Cations[a]			
Si	2.68	1.73	2.86
Al	2.78	0.92	0.96
Ca			
Mg	0.23	0.23	
Fe		1.39	0.00
K			0.01
Na	0.46	0.28	0.93
Mn		2.71	0.37

Normalized 100 wt%

[a] Cations based upon number of oxygens

[b] Total iron expressed as Fe^{3+}

[c] Total manganese expressed as Mn^{2+}

Despite measurement conditions designed to minimize the depth of penetration of the electron beam and the resultant x-ray generation volume, we cannot entirely rule out the influence of substrate minerals in the analysis. An alternative explanation for minor Al and Si in the varnish analysis is that nanoscale clay and other dust particles are intimately mixed with the nanoscale Mn-rich phase [8, 10]. In either case, given the negative correlation between Mn and Si ($R^2 = 0.55$) and the more weakly negatively correlated Fe–Si ($R^2 = 0.26$), one may estimate the composition of the Mn oxide film at a Si concentration of zero. An extrapolation of these two regressed correlations results in an estimated Mn/Fe ratio of ~20 for "pure" Mn-oxide rock varnish (Table 4).

Biological microstructures such as filaments 10 s–100 μm in length are present on the rock varnish and are rich in carbon and nitrogen (Fig. 14a, b). Higher resolution compositional imaging of such microbial microstructures indicates that some biological activity post-dates Mn-deposition (Fig. 14c).

Discussion

Manganese and iron rock varnishes have been noted to occur in a wide range of environmental settings from well-studied examples in deserts around the globe to less studied examples in rainforests of multiple continents, near active glaciers, and on rocks exposed in rivers [7]. Given the latter, it is perhaps not entirely surprising to learn of rock varnish formation in Washington, DC, which is in the humid subtropical zone according to the Köppen climate classification. Average total precipitation in Washington is ~1000 mm per year, or roughly ten times greater than that for an urban desert location, e.g., Las Vegas, NV.

Rock varnish on the Seneca sandstone described here shares certain similarities with desert varnish: (1) high luster, nearly metallic in places; (2) Mn-rich particle sizes in the nanometer range from <20 to 200 nm; (3) high enrichment in Mn as well as Pb, Cu, and Zn (Table 2); (4) deposition on a lithological substrate containing a low bulk concentration of Mn (Table 1); and (5) mineralogical association with Al-rich silicate dust minerals intimately mixed with the Mn-rich coating (Fig. 8c).

Despite these parallels, rock varnish on the Smithsonian Castle sandstone possesses differences relative to varnish formed in arid settings, namely: (1) Mn is found in two zones, [i] dispersed along grain boundaries and pores in the uppermost 200–250 μm of the rock surface, and [ii] thin and discontinuous surface deposits ≪1 μm in thickness or roughly three orders of magnitude thinner than typical desert varnish. In cross section it is difficult to measure, or even identify, a surface deposit; (2) deposits have no discernable vertically definable substructure as opposed to microstratified desert varnish described in the literature [8, 13]. Differences in both the thickness and lack of microstratigraphy may be attributed to the age disparity between the architectural varnish and those formed over geological periods of time. In this regard Smithsonian varnish may serve as an example of the earliest stage of desert varnish formation.

Varnish minerals are either poorly crystalline, present at levels below the detection limit for x-ray diffraction (~5 volume%), or possibly both. Previous researchers have encountered a similar lack of diffracted x-ray signal, even for more developed desert varnish where the coating is significantly more massive compared to samples in this study [8]. Many Mn oxides formed in nature, e.g., birnessite, are poorly crystalline in general, which may well have compounded our inability to collect structural information [21]. Transmission electron microscopy or synchrotron-based x-ray methods represent useful follow-up methods to characterize the rock varnish in this study [12, 22, 23].

The composition of the varnish likely represents multiple phases, a Mn-rich oxide and an Al-rich silicate mineral. The aluminous phase is either intimately mixed with Mn oxide or results from sampling a clastic mineral grain substrate. Unmixing the convolved chemistry by extrapolating negatively correlated Mn–Si and Fe–Si to a zero Si

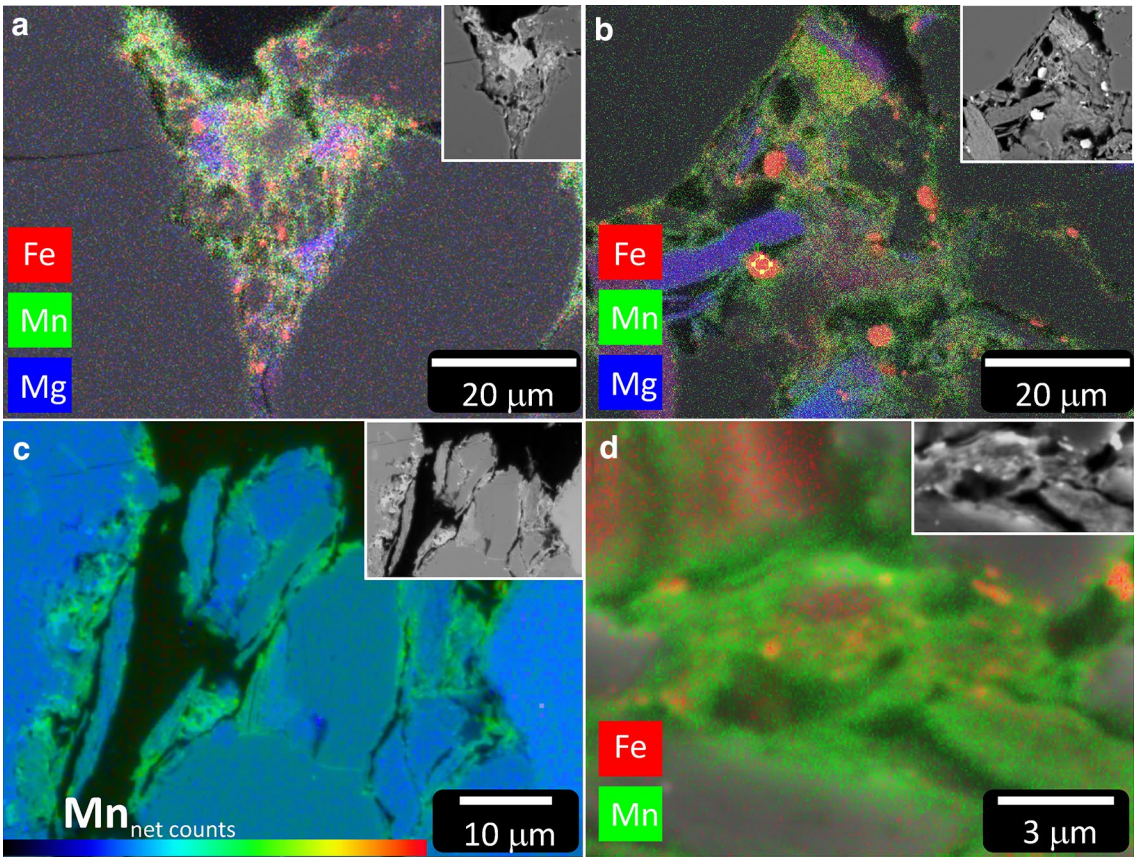

Fig. 9 X-ray imaging of Mn-rich zones in cross section. **a** and **b** Disposition of nanoscale-Mn-particle decorated surfaces within pores of the Seneca sandstone at moderate magnification. **c** Net count image of Mn Lα background subtracted and deconvolved from adjacent low energy peaks. **d** Nanoscale Mn and Fe oxides at higher magnification within a void. Backscattered electron images are *inset*

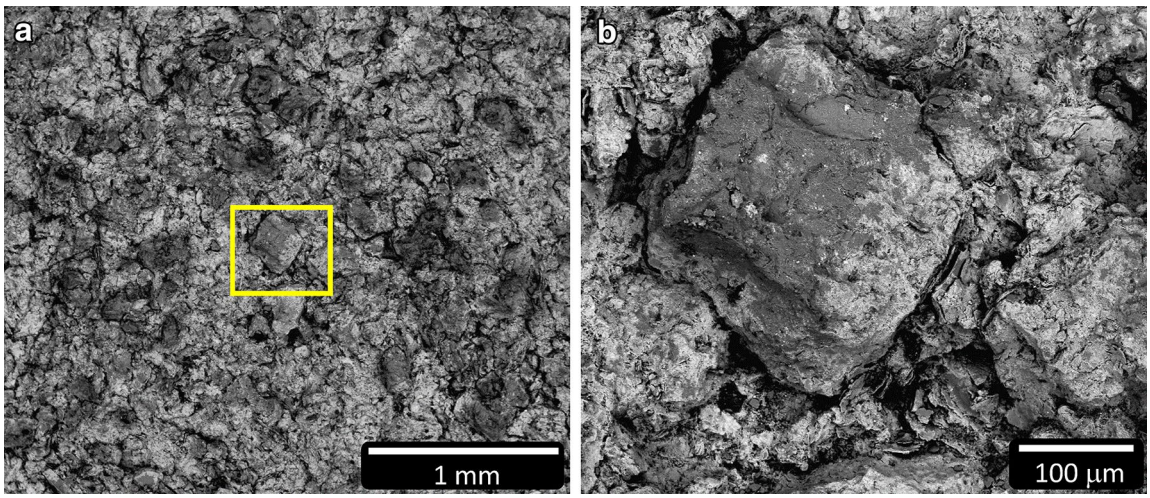

Fig. 10 Variable pressure SEM imaging of uncoated rock varnish surface. **a** Low magnification BSE image showing uneven average atomic number represented by *greyscale* intensity, at the millimeter scale; hence, *lightest* areas are enriched in Mn. **b** Close-up of partly Mn-coated sandstone grain highlighted in **a**

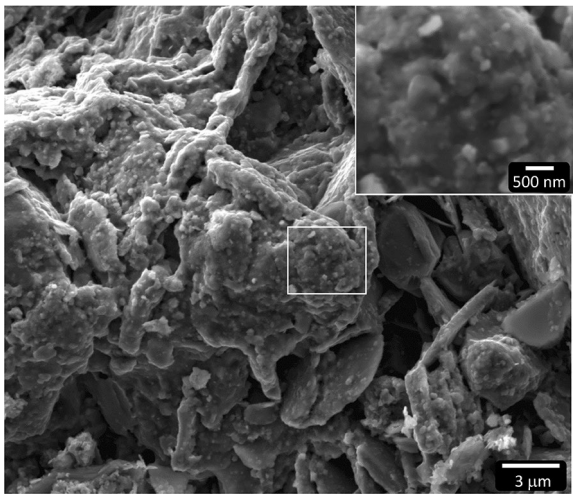

Fig. 11 Secondary electron (SE) image of Mn-rich rock varnish. *Inset*: Higher resolution SE image of nanoparticles in *highlighted* region

concentration end-member yields a Mn/Fe ratio of 20. Similar negative correlations between Si and Mn have been noted in desert varnish [8, 24]. The Mn-rich component within the nanophase mineral mixture is most likely either birnessite or todorokite.

Avg. composition: $Na_{0.2}Ca_{0.1}Mg_{0.1}Al_{0.1}Si_{0.5}Mn_{1.9}Fe_{0.5}O_{6.7}$

Birnessite: $(Na,\ Ca)_{0.5}\left(Mn^{4+},\ Mn^{3+}\right)_2O_4 \cdot 1.5H_2O$

Todorokite: $\left(Mn^{2+},\ Ca,\ Na,\ K\right)\left(Mn^{4+},\ Mn^{2+},\ Mg\right)_6O_{12} \cdot 3H_2O$

Potter and Rossman [9] found that different terrestrial weathering environments produced distinct mineralogy. If birnessite is the Mn-rich phase in the Smithsonian Castle varnish, the result is consistent with subaerial Mn varnish formed in stream deposits where birnessite is found in association with minor silicate minerals.

Apart from an extreme enrichment in Mn relative to the Seneca sandstone, the varnish is additionally concentrated in a number of heavy metals, including Pb, Zn, Cu, and Ni. These results are consistent with experiments that have determined divalent metal preferential adsorption for Pb, Zn, and Cu on interlayer crystallographic sites in birnessite [25]. Analytical studies also show a significant enrichment of Mn, Co, Pb, Ni, and Cu in desert varnishes [24, 26].

According to previous investigators, e.g., [7, 10], the mechanism of formation of Mn rock varnishes involves multiple steps: (1) accumulation of externally derived clay-bearing dust on a rock surface [10], (2) transport of Mn to the rock surface in solution within rain/fog droplets, and (3) oxidation and precipitation of Mn oxide cementing previously unconsolidated clay into a heterogeneous nanophase mixture. Step 1 was recently bolstered by the observation that anticorrelated Mn and Si electron microprobe analyses for desert varnish have a common Mn-free end-member regardless of the composition of the varnished rock [24]. Regarding step 2, one may question whether Mn is derived locally from the host rock or externally via atmospheric transportation [8]. In this study we report the presence of hematite, titanite, and rutile in the Seneca sandstone, which may all serve as internal reservoirs of Mn. However, to within the sensitivity of our compositional imaging we find no evidence for solution transportation of Mn in the sandstone.

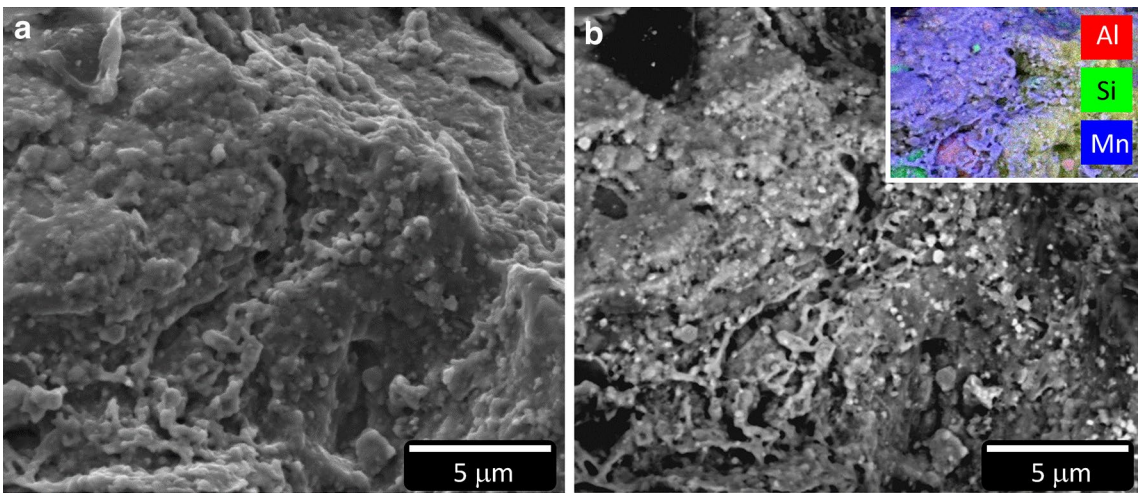

Fig. 12 Microstructural imaging of rock varnish. **a** SE image showing the morphology of a partly coated region of the rock surface. **b** BSE image depicting the average atomic number differences in the same area. *Inset*: Compositional overlay

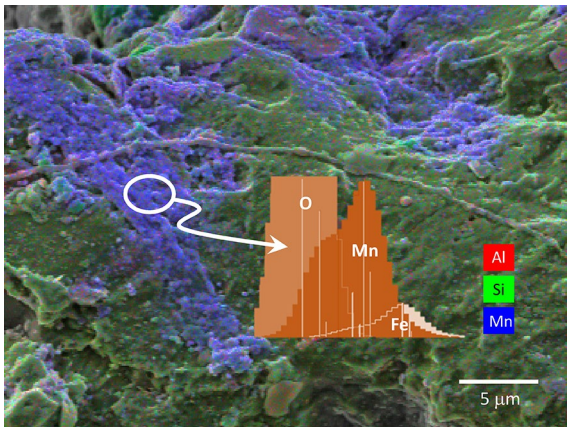

Fig. 13 Distribution of Mn in rock varnish. The composite x-ray image shows that Mn enrichment occurs in discrete discontinuous zones at the rock-atmosphere interface. Deconvolved low energy x-ray peaks show the relative contributions of Mn and Fe in the *highlighted* region

Based upon rare earth element fractionation observed in desert varnish it has been argued that the degree of element fractionation observed is inconsistent with isochemical leaching and reprecipitation within the same rock [26]. Therefore, the source of Mn must be delivered to the rock surface externally via atmospheric transport and surface leaching/dissolution of airborne dust grains. The final step 3 requires oxidation and precipitation of Mn either by a physiochemical process under acidic oxidized conditions in rainwater [26] or via microbially assisted oxidation as favored by other investigators [7, 11, 27]. The microstructural imagery collected on the Smithsonian Castle varnish offers no evidence for microbial entombment in Mn oxide, and the organisms observed on the surface (Fig. 14) grew upon the varnish and therefore may not be related to Mn oxidizing microbes. Apart from local compositional heterogeneity discussed above, another factor to consider regarding the likelihood of varnish development is stone roughness. Rougher areas provide increased surface area for condensation and therefore deposition of atmospheric dust. However, no systematic associations between surface roughness and rock varnish have been noted on the building stone and gateposts.

The patchy distribution of varnish on the Castle is less consistent with a chemical process, which would lead to the development of a more uniform coating, and more suggestive of biological colonization. It seems reasonable that biological mediation must play some significant role in Mn oxidation, if in tandem with abiological processes, in the development of rock varnishes in this study. Furthermore, we cannot state definitively why varnish formation is occurring on the Smithsonian Castle Seneca sandstone as opposed to other building stones on the National Mall. However, it has been noted that

> *"the irregular onset of bacterial colonization accounts for the puzzling inconsistency in varnish development from stone to stone..." [11].*

The rate of subaerially exposed Mn varnish formation in the western USA has been estimated to range between <1 and 40 nm/a [28]. Given that the age of the Castle gatepost exposure to the atmosphere is known to be just under 30 years, a rock varnish thickness range of ~28 nm–1.08 µm would be expected using the rates determined for the western USA. The observed surface coating is closer to the lowest end of that thickness range, although Mn-rich particles sequestered in pores within the sandstone do not contribute to the surface thickness estimate. A rare 20–40 year old rock varnish has been

Table 4 SEM-based x-ray microanalysis results for carbon coated rock varnish extracted from Mn-rich zones expressed as atomic per cent

Element	O	Na	Mg	Al	Si	Mn	Fe	Ca	Mn/Fe
X-ray line	K_α	K_α	K_α	K_α	K_α	L_α	L_α	K_α	
RV 1	65.8	1.9	1.3	1.2	3.9	22.5	3.2	0.4	7.0
RV 2	66.7	1.9	1.7	1.6	5.6	18.0	4.4	0.1	4.1
RV 3	65.7	1.5	1.0	2.4	6.5	14.1	8.9		1.6
RV 4	67.0	1.9	1.4	1.2	4.4	19.4	4.3	0.4	4.6
RV 5	67.0	1.9	1.4	1.4	5.8	18.1	4.0	0.4	4.5
RV 6	67.0	1.9	1.4	1.2	4.4	19.4	4.3	0.4	4.6
RV 7	68.4	1.3	1.0	0.8	3.3	17.7	6.6	0.8	2.7
RV 8	68.5	1.7	1.2	0.7	2.8	21.5	2.9	0.8	7.4
Average	67.0	1.8	1.3	1.3	4.6	18.8	4.8	0.5	4.5
St dev	1.0	0.2	0.2	0.5	1.2	2.4	1.8	0.2	1.8
Calc. Si = 0					0.0	25.6	1.3		20.2

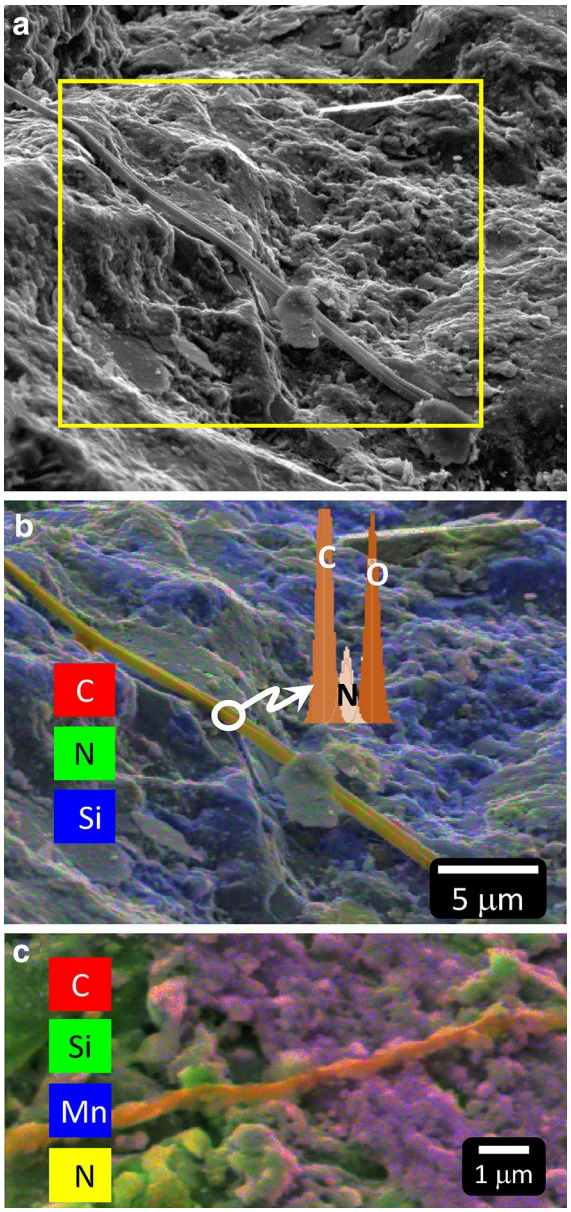

Fig. 14 Microbiological activity on rock varnish. **a** SE image depicting a long (many 10 s of microns) filament attached to the sandstone surface. **b** X-ray image overlay of *highlighted* region in **a**. **c** Higher resolution SEM-based compositional image showing microbial microstructure over Mn-rich rock varnish on a gatepost sample

reported forming on steel slag piles in southern California [29], where the substrate material is rich in Mn, possibly influencing the rapid rate of growth. Impressively, in a few short decades stone disfigurement of the Smithsonian's Castle is readily noticeable and a testament to the strong pigmentation of Mn oxides even when present in small concentrations.

Removal of varnish from the stone may prove problematic. While laser cleaning can be used to remove the exposed coating it will be more difficult to remove Mn oxide within pores without damaging the sandstone.

Conclusions

Rock varnish on Smithsonian Castle is comprised of a discontinuous thin film (≪1 μm) of Mn-rich and Al-rich silicate nanoparticles on Seneca sandstone. Mn-rich particles range from <20 to 200 nm in size. The nanoscale mixture also decorates the grain boundaries and cavities of the uppermost 100–250 μm of the rock-atmosphere interface, strongly altering the color of the red stone to lustrous black despite the relatively small mass of the deposits.

The varnish is poorly crystalline and has an estimated composition of $Na_{0.2}Ca_{0.1}Mg_{0.1}Al_{0.1}Si_{0.5}Mn_{1.9}Fe_{0.5}O_{6.7}$. It is likely that this Mn-rich composition represents an intimate mixture of a Mn oxide, e.g., birnessite or todorokite, and Al-rich silicate dust. The Mn/Fe ratio of the Mn-rich end-member is estimated to be ~20.

The rock varnish on the Smithsonian Castle is both thinner than typical desert varnish by a factor of 100 s–1000× and lacks microstratigraphy. Both differences may be accounted for by the much younger age of the architectural varnish compared to varnish deposits formed over glacial to geological time frames. A significant mass of Mn-oxide is held more deeply below the rock surface (within the upper 250 μm), principally along mineral surfaces within pores, which complicates estimates for the rate of Smithsonian varnish formation.

Abbreviations

Afs: alkali feldspar; Ap: apatite; Bt: biotite; Cly: clay; Hem: hematite; μm: micrometer; nm: nanometer; Pl: plagioclase; Sst: sandstone; Ttn: titanite; Qtz: quartz.

Authors' contributions

EPV conducted laboratory-based portable XRF measurements and data analysis, collected all scanning electron and x-ray spectroscopic imagery, and performed all data analysis and interpretation. CAG coordinates the research project on rock varnish of the Seneca sandstone at the Smithsonian, performed field and studio photography, and provided the historical architectural context for the study. RAL first recognized the significance of the black patches while conducting a separate investigation on the properties of building stone and has led other studies of the problem. ZW-Y performed photography, researched buildings in the Washington, DC, region built of Seneca sandstone, and annotated architectural elevations showing the location of the black patches. EPV wrote the paper with input from CAG and RAL. All authors read and approved the final manuscript.

Authors' information

EPV is a research scientist at Smithsonian's Museum Conservation Institute and president of the International Union of Microbeam Analysis Societies. Since 1984, CAG has been Senior Objects Conservator at the Smithsonian Institution, where she has been particularly concerned with the conservation of artifacts and buildings made of stone. RAL has been involved with

stone conservation since 1978. ZW-Y is an undergraduate at the University of Maryland majoring in art history, who participated in the project as a summer intern.

Author details
[1] Smithsonian Institution, Museum Conservation Institute, 4210 Silver Hill Road, Suitland, MD 20746, USA. [2] Department of Materials Science and Engineering, University of Maryland, 2135 Chemical & Nuclear Engineering Bldg #090, College Park, MD 20742, USA.

Acknowledgements
We would like to thank Emily Aloiz, who initially analyzed the Seneca sandstone and documented its condition; Jennifer Giaccai, Willa Freedman, and Gwénaëlle Kavich, who performed the field-based XRF analyses of the Smithsonian Castle rock varnish; and Melvin Wachowiak, who collected light microscopy images. EPV acknowledges the Materials Measurement Science Division of the National Institute of Standards and Technology, where he performed some of the electron microscopy presented here as a guest researcher. We also thank the Smithsonian's Museum Conservation Institute for generous support for the project.

Competing interests
The authors declare that they have no competing interests.

Received: 4 September 2015 Accepted: 26 June 2016
Published online: 22 July 2016

References

1. Hafertepe K. America's Castle: the evolution of the Smithsonian building and its institution, 1840–1878. Washington, DC: Smithsonian Institution Press; 1984.
2. Ewing HP, Ballard A. A guide to Smithsonian architecture. Washington, DC: Smithsonian Books; 2009.
3. Peck G. The Smithsonian Castle and the Seneca Quarry. Charleston: The History Press; 2013.
4. Owen RD. Hints on public architecture: containing, among other illustrations, views and plans of the Smithsonian Institution. New-York: G. P. Putnam; 1849.
5. Report of the Board of Regents of the Smithsonian Institution. Congressional serial set 30th Congress [Senate], 1st Session, Miscellaneous Document No. 23: United States Government Printing Office; 1848. p. 5.
6. Grissom CA, Vicenzi EP, Livingston RA, Aloiz E, Little N, Giaccai J, et al. Manganese in black crusts on Seneca sandstone. Microsc Microanal. 2014;20:2044–5.
7. Dorn RI, Oberlander TM. Rock varnish. Prog Phys Geogr. 1982;6:317–66.
8. Potter R, Rossman G. The manganese- and iron-oxide mineralogy of desert varnish. Chem Geol. 1979;25:79–94.
9. Potter RM, Rossman GR. Mineralogy of manganese dendrites and coatings. Am Mineral. 1979;64:1219.
10. Potter RM, Rossman GR. Desert varnish: the importance of clay minerals. Science. 1977;196:1446–8.
11. Dorn RI, Oberlander TM. Microbial origin of desert varnish. Science. 1981;213:1245–7.
12. Krinsley D, Dorn R, Tovey NK. Nanometer-scale layering in rock varnish: implications for genesis and paleoenvironmental interpretation. J Geol. 1995;103:106–13.
13. Liu T, Broecker WS. Rock varnish microlamination dating of late quaternary geomorphic features in the drylands of western USA. Geomorphology. 2008;93:501–23.
14. Dietzel M, Dietzel M, Kolmer H, Polt P, Simic S. Desert varnish and petroglyphs on sandstone—geochemical composition and climate changes from Pleistocene to Holocene (Libya). Chemie der Erde. 2008;68:31–43.
15. Goldsmith Y, Goldsmith Y, Stein M, Enzel Y. From dust to varnish: geochemical constraints on rock varnish formation in the Negev Desert, Israel. Geochimica et cosmochimica acta. 2014;126:97–111.
16. Kim SS, Bargar JR, Nealson KH, Flood BE. Searching for biosignatures using electron paramagnetic resonance (EPR) analysis of manganese oxides. Astrobiology. 2011;11:775–86.
17. Glascock MD, Neff H. Neutron activation analysis and provenance research in archaeology. Meas Sci Technol. 2003;14:1516.
18. Kotula PG, Keenan MR, Michael JR. Automated analysis of SEM X-ray spectral images: a powerful new microanalysis tool. Microsc Microanal. 2003;9:1–17.
19. Keenan MR. Exploiting spatial-domain simplicity in spectral image analysis. Surf Interface Anal. 2009;41:79–87.
20. Aloiz E, Grissom CA, Davis JM, Livingston RA. Characterization of the Smithsonian Institution's building stones using conventional and advanced analytical methods. In: Proceedings, 12th international congress on deterioration and conservation of stone. 2015.
21. Post JE. Manganese oxide minerals: crystal structures and economic and environmental significance. Proc Natl Acad Sci USA. 1999;96:3447–54.
22. Post JE, Veblen DR. Crystal-structure determinations of synthetic sodium, magnesium, and potassium birnessite using tem and the Rietveld method. Am Mineral. 1990;75:477–89.
23. McKeown DA, Post JE. Characterization of manganese oxide mineralogy in rock varnish and dendrites using X-ray absorption spectroscopy. Am Mineral. 2001;86:701–13.
24. Macholdt DS, Jochum KP, Pöhlker C, Stoll B. Microanalytical methods for in situ high-resolution analysis of rock varnish at the micrometer to nanometer scale. Chem Geol. 2015;411:57–68.
25. Manceau A, Lanson B, Drits VA. Structure of heavy metal sorbed birnessite. Part III: results from powder and polarized extended X-ray absorption fine structure spectroscopy. Geochim Cosmochim Acta. 2002;66:2639–63.
26. Thiagarajan N, Lee CTA. Trace-element evidence for the origin of desert varnish by direct aqueous atmospheric deposition. Earth Planet Sci Lett. 2004;224:131–41.
27. Tebo BM, Bargar JR, Clement BG, Dick GJ. Biogenic manganese oxides: Properties and mechanisms of formation. Annu Rev Earth Planet Sci. 2004;32:287–328.
28. Liu T, Broecker WS. How fast does rock varnish grow? Geology. 2000;28:183–6.
29. Dorn RI, Meek N. Rapid formation of rock varnish and other rock coatings on slag deposits near Fontana, California. Earth Surf Process Landf. 1995;20:547–60.